Photonics and Optoelectronics

Design for Manufacturability (DFM) Models, Methods, and Tools for Silicon Photonics

S. I. El-Henawy, G. Martinez, D. Moon, M. B. McIlrath, D. S. Boning
Sponsorship: AIM Photonics

Silicon photonics, where photons instead of electrons are manipulated, shows promise for higher data rates, lower energy communication and information processing, biomedical sensing, Lab-On-A-Chip, and novel optically based functionality applications such as wavefront engineering and beam steering of light. In silicon photonics, both electrical and optical components can be integrated on the same chip, using a shared silicon integrated circuit (IC) technology base. However, silicon photonics does not yet have mature process, device, and circuit variation models for the existing IC and photonic process steps; this lack presents a key challenge for design in this emerging industry.

Our goal is to develop key elements of a robust design for manufacturability (DFM) methodology for silicon photonics. This design includes using statistical modelling to capture manufacturing variations, both systematic and random, at the wafer, chip, or feature scales and predicting their impact on photonic device and circuit levels. These variation-aware models and methods will help enable tomorrow's silicon photonics designers to predict and optimize behavior, performance, and yield of complex silicon photonic devices and circuits, just as IC designers do today.

To achieve this goal, we model the process variation effects, such as side wall verticality and edge roughness (Figure 1), on the optical behavior represented in the refractive index (Figure 2) or transmitted power variation in a splitter device (Figure 3). Also, we carry out Monte Carlo simulations in which the geometric variations for the optical components are simulated with Gaussian distributed variations and the resulting probability distribution functions (pdfs) for losses and the refractive index are calculated. Such models and simulations for different active and passive optical components will help to provide variation-aware models and methods for emerging process design kits for silicon photonic technologies.

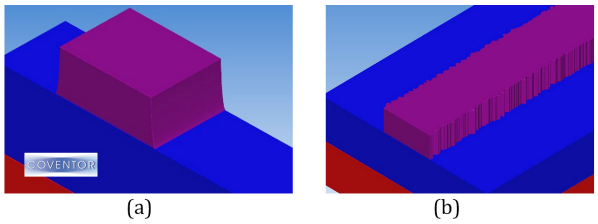

▲Figure 1: Effect of process variation on a silicon waveguide structure over oxide; (a) side wall verticality, (b) edge roughness.

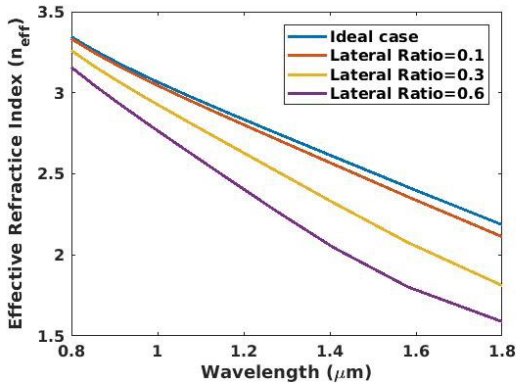

▲Figure 2: Effect of sidewall verticality variation on waveguide refractive index.

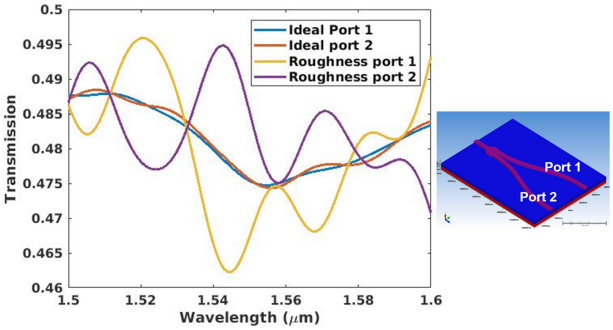

▲Figure 3: Effect of Gaussian edge roughness on Y-Branch transmission in the two different branches; imbalance is seen with roughness.

FURTHER READING

- L Chrostowski and M. Hochberg, *Silicon Photonics Design: from Devices to Systems*, Cambridge: Cambridge University Press, 2015.
- J. E. Bowers, T. Komljenovic, M. Davenport, J. Hulme, A. Y. Liu, C. T. Santis, A. Spott, S. Srinivasan, E. J. Stanton, and C. Zhang, "Recent Advances in Silicon Photonic Integrated Circuits," *SPIE OPTO, International Society for Optics and Photonics*, San Francisco, CA, 977402-977402, Feb. 2016.

Stochastic Simulation and Robust Design Optimization of Integrated Photonic Filters

T. W. Weng, D. Melati, A. Melloni, L. Daniel
Sponsorship: NSF

Photonics is rapidly emerging as a mature and promising technology, and it is evolving from a pure research topic to a market-ready player, aiming at achieving large production volumes and low fabrication costs. Pushed by these motivations, Process Design Kits, circuit simulators, generic foundry approaches, and multi-project-wafer runs are quickly changing the way that photonic circuits are conceived and designed. On the other hand, stochastic uncertainties such as fabrication variations are unavoidable in production processes. It is well known that such uncertainties can have a dramatic impact on the functionality of fabricated circuits. In order to obtain a high quality design of a photonic circuit, it is important to include such uncertainties during the early design stages. Hence, uncertainty quantification techniques become fundamental instruments to efficiently obtain the statistical information and to achieve a high-quality design.

Monte Carlo simulation is commonly exploited to evaluate the impact of fabrication uncertainties on the functionality of the designed circuits. Although effective, it suffers from a slow convergence rate and requires a long computation time. Meanwhile, stochastic spectral methods have recently been regarded as a promising alternative for statistical analysis due to their fast convergence. The key idea is to approximate the output quantity of interest (e.g., the bandwidth of a filter) with a set of orthonormal polynomial basis functions, known as generalized polynomial chaos expansion. Our goal in this work is to develop an efficient, robust design-optimization technique based on the state-of-the-art sampled-based stochastic spectral methods, which are mainly used for statistical analysis in the field of uncertainty quantification. Figure 1 shows a fifth-order directly coupled ring resonator used to demonstrate our technique. Due to fabrication process variations, the gap g and effective phase index neff of each ring resonator are uncertain, so the 3dB bandwidth varies greatly. In this example, we would like to design the nominal gap g for each ring that minimizes the mean-square-error of 3dB bandwidth. Figure 2 plots simulation results of the un-optimized nominal design and optimized nominal design. We show that the optimized circuits are more robust to fabrication process variations and achieve a reduction of 11 % to 35 % in the mean-square-errors of the 3dB bandwidth than un-optimized nominal designs.

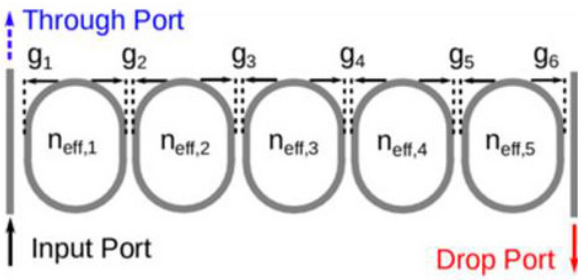

▲ Figure 1: A 5-ring coupled resonator.

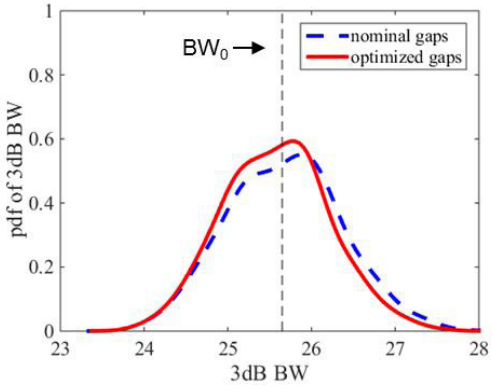

▲ Figure 2: Probability density functions of 3dB. Bandwidth of the un-optimized nominal design (blue dash line) and optimized nominal design (red line).

FURTHER READING

- D. Melati, A. Alippi, and A. Melloni, "Waveguide-Based Technique for Wafer-Level Measurement of Phase and Group Effective Refractive Indices," *J. Lightwave Technology*, vol. 34, no. 4, 1293-1299, 2016.
- D. Xiu and G.E. Karniadakis, "Modeling Uncertainty in Flow Simulations via Generalized Polynomial Chaos," *J. Computational Physics*, vol. 187, 137-167, 2003.

Visible Wavelength Integrated Modulators using Hybrid Waveguides

K. K. Mehta, G. N. West, R. J. Ram
Sponsorship: NSF, Lincoln Laboratory

Infrared integrated optics has proven useful for reducing system size, cost, and complexity for instruments from classical computers to sensors. Visible wavelength integrated photonic devices were the logical next step but common visible waveguides lack the ability to modulate light. We use a hybrid silicon nitride/lithium niobate (SiN/LN) platform to demonstrate visible-wavelength (674 nm) integrated waveguides and Mach-Zehnder-type modulators. The waveguides have propagation loss of ~4.0 dB/cm, and the MZMs were measured to have V_π = 3.0V.

Lithium niobate is one of the most commonly used electro-optically tunable materials for devices such as telecom modulators, due to its large r_{33} tensor component (~31 pm/V). Unfortunately, fabrication methods for directly etching lithium niobate are poor—argon ion etching is the method of choice, but it leaves rough, sloped sidewalls poorly suited to integrated photonic devices. We use the "hybrid" approach, where a layer of high-index material (silicon nitride, ~160 nm) is deposited on top of a thin film of lithium niobate (~215 nm) and patterned using electron beam lithography. The mode effective index around this silicon nitride ridge is then higher than the slab mode, leading to optical confinement. As the mode intensity largely exists inside the lithium niobate, direct electro-optic tuning is achievable.

Tested MZMs had 1 mm and 3 mm modulation lengths (Figure 1a) with Ti/Au contacts in a push-pull configuration deposited directly on the surface of the lithium niobate. The measured extinction was >20 dB. The measured V_π is lower than the voltage predicted by calculations of the mode confinement and applied field, likely due to a contribution from the piezoelectric properties of lithium niobate at low frequencies (Figure 1b).

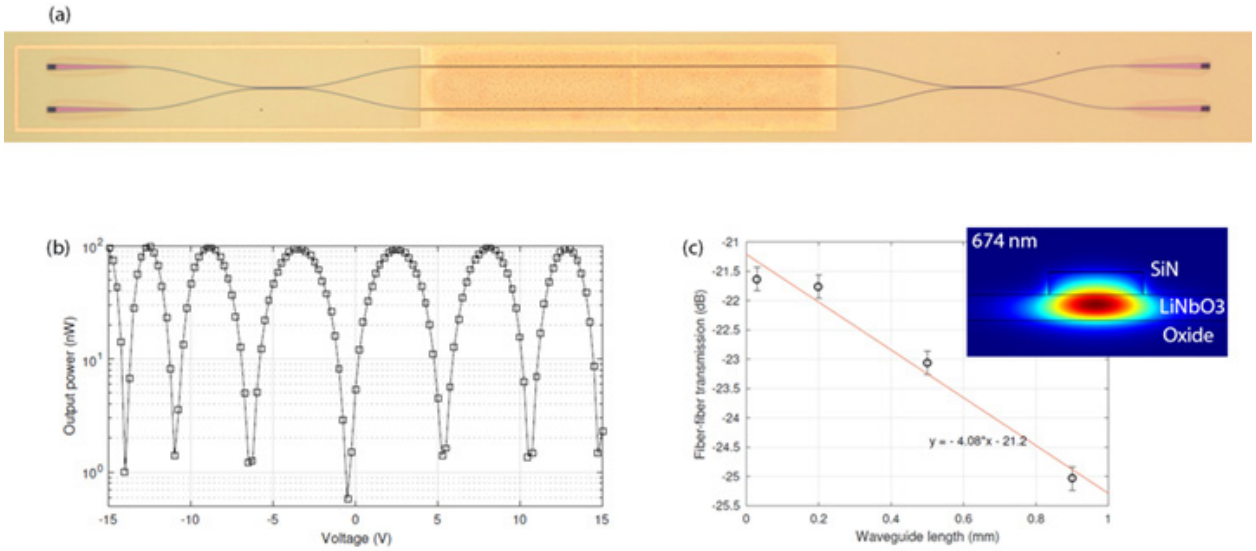

▲ Figure 1: (a) Optical micrograph of a Mach-Zehnder-type modulator, with an actively modulated length of 1 mm, (b) power transmission as a function of voltage for a tested device, showing a V_π of 3.0V near zero bias, (c) loss of straight waveguide test structures. Inset: Simulated mode profile in the waveguide cross section.

FURTHER READING

- A. Rao, A. Patil, J. Chiles, M. Malinowski, S. Novak, K. Richardson, P. Rabiei, and S. Fathpour, "Heterogeneous Microring and Mach-Zehnder Modulators Based On Lithium Niobate and Chalcogenide Glasses On Silicon," *Optics Express*, vol. 23, no. 17, 22746-22752, 2015.
- K. K. Mehta, C. D. Bruzewicz, R. McConnel, R. J. Ram, J. M. Sage, and J. Chiaverini, "Integrated Optical Addressing of an Ion Qubit," *Nature Nanotechnology*, vol. 11, 1066-1071, 2016.

Visible Integrated Photonics in Microelectronic CMOS

A. H. Atabaki, G. N. West, R. J. Ram
Sponsorship: DARPA

Despite numerous advances in visible/near-infrared (VIS/NIR) integrated photonic devices and platforms, less progress has been made toward scalable VIS/NIR platforms that integrate active and passive photonic devices (e.g., waveguides, resonators, and photodetectors). Many VIS/NIR optical applications, from sensing to quantum information processing, require a combination of optical functions from optical addressing and detection to modulation and filtering. Our ability to envision new systems and architectures for these applications hinges on integrated photonic platforms that enable these functions in a scalable fashion. Such platforms are essential to provide the combination of design flexibility and scale-up needed for the next generation of sensing, imaging, and quantum information processing systems.

In this work, our goal is to develop a powerful integrated photonic platform for UV/VIS/NIR wavelengths by implementing passive and active photonic devices monolithically with electronics in a standard complementary metal-oxide semiconductor (CMOS) process. We design all of our devices in CMOS, and implement the passive structures through backend processing of the CMOS chips. Our devices are fabricated in a 300-mm CMOS foundry using IBM's 65-nm bulk CMOS process (Figure 1a). We use the shallow-trench isolation (STI) mask with deep-sub-micron lithography resolution to define a template in the silicon substrate for subsequent incorporation of the passive devices. The CMOS die is flip-chip bonded on a handle, and the silicon under the passives is removed in the XeF2 etcher. The remaining oxide template is then isotropically filled with 200 nm of Al_2O_3 with atomic layer deposition (ALD) at 120°C. Figures 1a and 1b show the CMOS device and waveguide fabrication process. We also repurposed the transistor gate polysilicon to design very compact grating couplers (Figure 1a). Figure 1c shows light guiding at red and violet in these backend waveguides. Our approach avoids any lithography in post processing, which simplifies fabrication and guarantees perfect alignment of all devices.

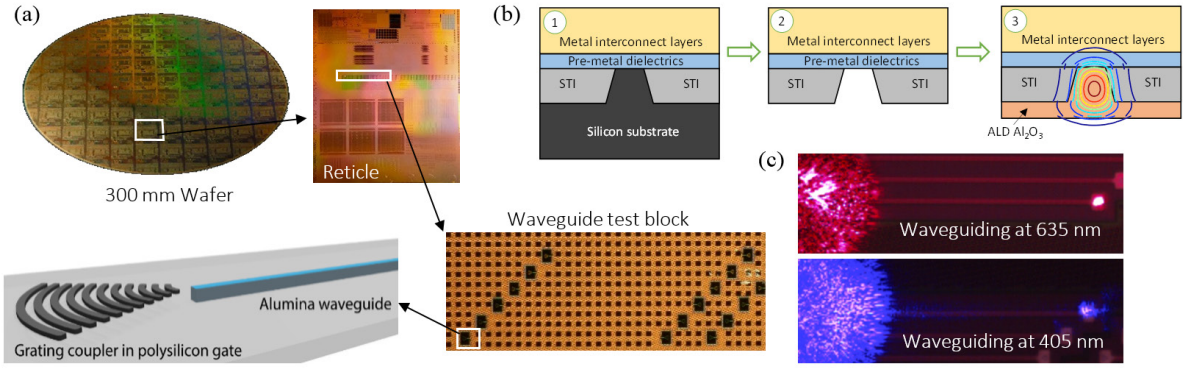

▲Figure 1: (a) Photos of the wafer and reticle and micrograph of the waveguide test block. Schematic of the polysilicon grating couplers and waveguide structure shown on the left, (b) backend fabrication steps for VIS waveguides. E-field of the fundamental Transverse Electric (TE) mode is overlaid on panel 3, (c) micrographs of the chip with red and violet light coupled into the Al_2O_3 waveguides. Bright light on the right side of the photos is the guided light radiated out of the chip.

FURTHER READING

- S. Romero-García, F. Merget, F. Zhong, H. Finkelstein, and J. Witzens, "Silicon Nitride CMOS-Compatible Platform for Integrated Photonics Applications at Visible Wavelengths," *Opt. Express*, vol. 21, 14036-14046, 2013.
- K. K. Mehta, C. D. Bruzewicz, R. McConnell, R. J. Ram, J. M. Sage, and J. Chiaverini, "Integrated Optical Addressing of an Ion Qubit," *Nature Nanotechnology* doi:10.1038/nnano.2016.139, 2016.
- J. S. Orcutt, B. Moss, C. Sun, J. Leu, M. Georgas, J. Shainline, E. Zgraggen, H. Li, et al, "Open Foundry Platform for High-Performance Electronic-Photonic Integration," *Optics Express*, vol. 20, 12222-12232, 2012.

SiC-on-Insulator-on-Chip Photonic Device in a Radiative Environment

D. Ma, Z. Han, Q. Du, J. Hu, L. Kimerling, A. Agarwal
Sponsorship: DTRA

Silicon carbide (SiC) has played significant roles in a variety of electronic and photonic devices in the past decade due to its excellent properties including high irradiation tolerance, stability despite exposure to high temperatures and harsh chemicals, high thermal conductivity, and high Young's modulus. SiC is a good candidate material for on-chip microphotonics because of its high refractive index, large band gap, and complementary metal-oxide semiconductor (CMOS) compatibility. SiC can serve in both active and passive photonic device components. The CMOS compatibility of SiC enables low-cost device processing and scalable industrial applications, highlighting its advantage over other large band gap non-CMOS–compatible semiconductors.

A plasma enhanced chemical vapor deposition (PECVD) system using a silane and methane gas mixture has been used to deposit an amorphous SiC layer on a 6-inch Si wafer with a top layer of 3-micron thermal oxide (Silicon Quest International, Inc.). To pattern and fabricate the SiC-on-insulator photonic device (a resonator), a chromium metal mask was used. Fluorine chemistry was used to dry etch SiC using reactive ion etching. The etch parameters were optimized to enhance the etch rate while still delivering low-loss sidewall profiles as shown in Figure 1.

The effect of gamma irradiation on a SiC resonator was investigated by measuring its quality factor before and after exposing the device to high dose (60 Mrad) gamma irradiation. The quality factor maintained the same order of magnitude, and the resonant peak at critical coupling remained in the near IR range as shown in Figure 2. Both these results demonstrate the gamma irradiation tolerance of the SiC-on-insulator photonic device.

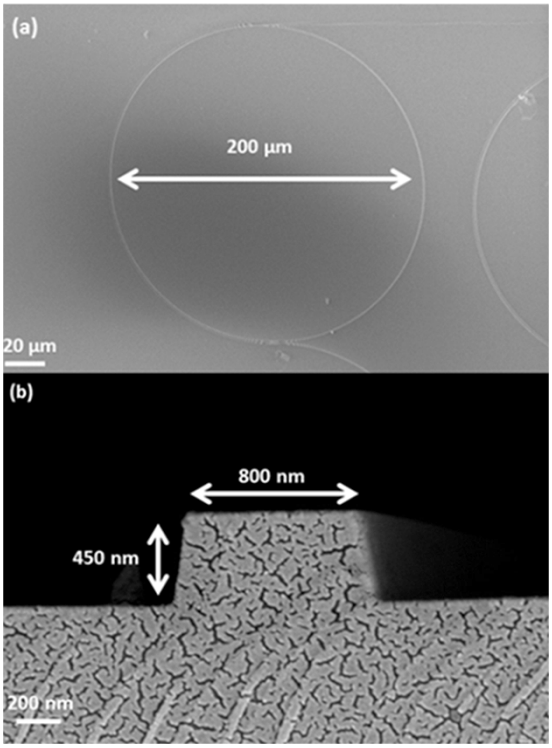

▲Figure 1: Scanning electron microscopic images of (a) the top view and (b) the cross section of the SiC-on-insulator device. (The texture on the cross-section image was due to the gold conductive coating for better image resolution.)

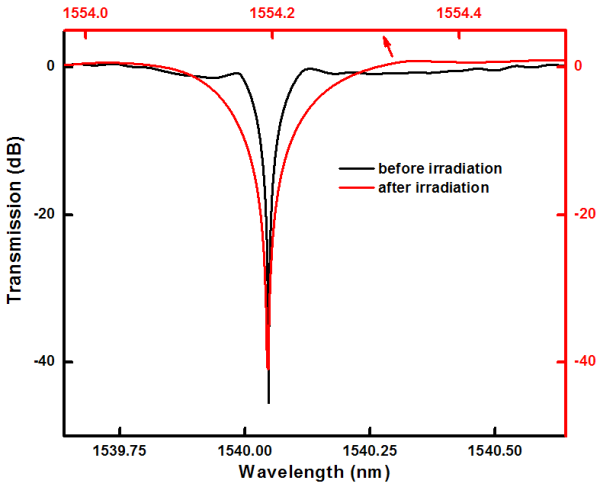

▲Figure 2: Comparison of the resonant peak before (black) and after (red) 60 Mrad gamma irradiation.

FURTHER READING

- D. Ma, Z. Han, Q. Du, J. Hu, L. Kimerling, A. Agarwal, and D. T. H. Tan, "SiC-on-Insulator On-Chip Photonic Sensor in a Radiative Environment," *Sensors*, IEEE, 1-3, 2016.

Germanium Electroabsorption Modulator for Silicon Photonic Integration

D. Ma, L. C. Kimerling, J. Michel
Sponsorship: Futurewei Technologies, Inc.

Photonic modulators on Si substrate with high speed and low energy consumption are important components for integrated photonics. The Ge-on-Si system provides an opportunity for integrated electro-absorption modulators that turn the material from transparent to opaque in the working wavelength regime under an applied electric field. Although Ge is an indirect gap semiconductor, its energy difference between the direct gap and indirect gap is as small as 136 meV. The direct band gap of 0.8 eV corresponds to a wavelength of 1550 nm, which is the most technically important wavelength in optical communications and the most commonly used in Si photonics.

The fast speed and low energy consumption of the Ge modulator require high-quality Ge on Si heteroepitaxy. The threading dislocation density, as well as film crystallization and composition, were monitored and controlled. During the ultrahigh vacuum chemical vapor deposition, a constant-composition buffer layer was first deposited at low temperature. Despite the large lattice mismatch, the buffer layer is planar due to limited surface-diffusion, which prevents surface islanding. The buffer layer thickness was optimized to maintain high film quality, on which the high quality Ge epitaxial film was grown at high temperature followed by thermal annealing.

The Si photonic integrated Ge modulator was designed with efficient light coupling from the Si waveguide to the Ge modulator using a Ge taper structure. The effect of taper dimensions on the insertion loss of modular was evaluated in a finite element model and considered in the device fabrication. Insertion loss is the major source of loss when the light signal is transferred from the Si waveguide to the Ge modulator. A fabrication process using electron beam lithography and chemical dry etching has been developed. The pattern formed by the photoresist was transferred using reactive ion etching (REI) to fabricate the Ge taper, which produced a tapered tip with sidewall angle of 100 degrees. A gradually sloped taper tip might improve the coupling efficiency between the Si and Ge components and lower the insertion loss of the modulator because the light couples more effectively through a medium with a gradually changing refractive index.

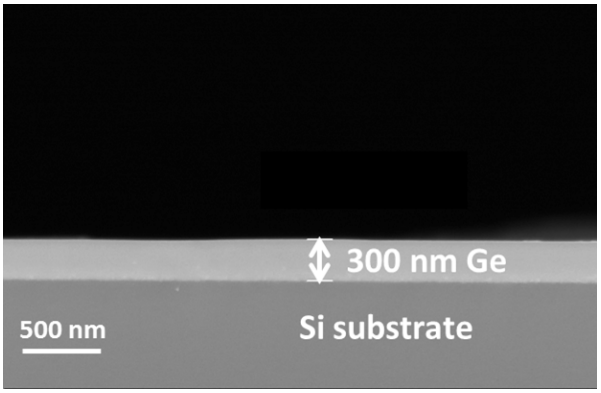

▲ Figure 1: Cross-sectional view, scanning electron microscopy (SEM) image of epitaxial Ge layer on Si substrate.

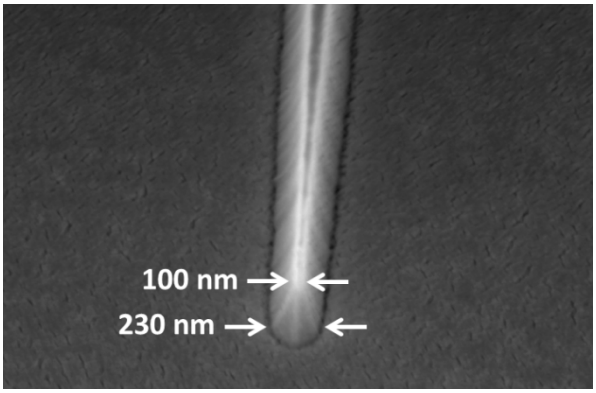

▲ Figure 2: Top-front view SEM image of taper tip fabricated via REI.

Surface-Plasmon-Induced Anisotropic Hot Electron Momentum Distribution in a Metallic-Semiconductor Photonic Crystal

X. H. Li, J. Chou, W. L. Kwan, A. El-Faer, S.-G. Kim
Sponsorship: Masdar Flagship Program

Metallic-semiconductor Schottky hot carrier devices have been found to be a promising solution for harvesting photons with energy lower than the bandgap of semiconductors, which is of crucial importance for realizing efficient solar energy conversion. In recent years, extensive efforts have been devoted to utilizing surface plasmon resonance to improve light absorption of devices by creating strong light-metallic-nanostructure interaction, which generates hot electrons through non-radiative decay. However, how surface plasmon enhances the efficiency of hot electron collection is still debatable.

We recently reported a metallic-semiconductor photonic crystal (MSPhC) with 2D nano-cavity arrays for photochemical energy conversion, which showed a sub-bandgap photoresponse centered at the surface plasmon polariton (SPP) resonance wavelength. Here we developed a theoretical model of internal photoemission in this device by incorporating the effects of anisotropic hot electron momentum distribution caused by SPP. As shown in Figure 1, the structure could generate SPP at the Au/TiO_2 interface along the sidewall of the nano-cavity, with resonance wavelength of 590 nm (photon energy of 2.1 eV). Near resonant wavelength, surface plasmon dominates the electric field in the thin Au layer, which generates hot electrons with high-enough momentum preferentially normal to the Schottky interface, as shown in Figure 2a. The influences of interband and intraband transition and SPP are incorporated to model the internal quantum efficiency of this device, as shown in Figure 2b. The anisotropic hot electron momentum distribution largely enhances the IQE and photoresponse near SPP resonance wavelength. Compared with the widely used Fowler's theory of Schottky internal photoemission, our model can better predict IQE of surface-plasmon-assisted hot electron collection. Combined with large-scale photonic design tools, this quantum-level model could be applied for tuning and enhancing the photoresponse of Schottky hot carrier devices.

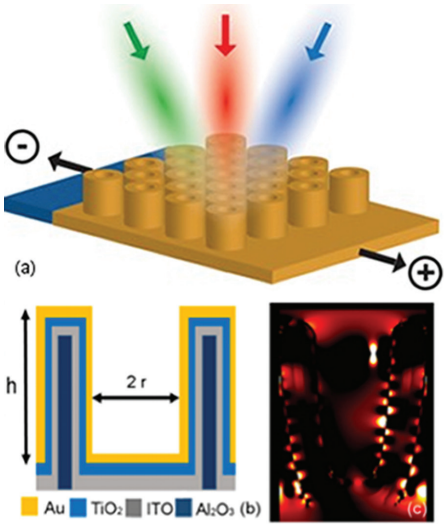

▲ Figure 1: (a) Schematic of the metallic-semiconductor photonic crystal with 2D nano-cavity array, (b) Schematic of the cross-section of MSPhC, (c) SPP at the Au/TiO_2 interface along the cavity sidewall at 590 nm, obtained from FDTD simulation.

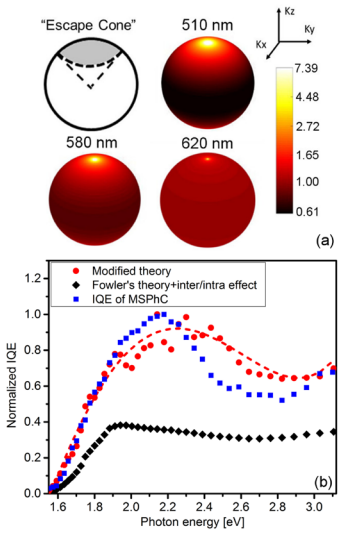

▲ Figure 2: (a) Anisotropic hot electron momentum distribution caused by SPP. SPP enhances distribution of hot electrons inside the "escape cone" on internal photoemission, (b) Comparison of our model and Fowler's theory on predicting IQE of MSPhC.

FURTHER READING

- J. B. Chou, X. H. Li, Y. Wang, D. P. Fenning, A. El-Faer, J. Viegas, M. Jouiad, S.-H. Yang, and S.-G. Kim, "Surface Plasmon Assisted Hot Electron Collection in Wafer-Scale Metallic-Semiconductor Photonic Crystals," *Opt. Express,* vol. 24, A1234-A1244, 2016.
- X. H. Li, J. B. Chou, W. L. Kwan, A. El-Faer, and S.-G. Kim, "Effect of Anisotropic Electron Momentum Distribution of Surface Plasmon on Internal Photoemission of a Schottky Hot Carrier Device," *Opt. Express* vol. 25, A264-A273, 2017.

Light-Emitting Surfaces with Tailored Emission Profile for Compact Dark-Field Imaging Devices

C. Chazot, C. J. Rowlands, R. J. Scherer, I. Coropceanu, Y. Kim, K. Broderick, S. Nagelberg, P. So, M. Bawendi, M. Kolle
Sponsorship: MTL, MISTI

Dark field microscopy is a well-known imaging technique used to enhance the contrast in unstained samples by suppressing low spatial frequency contributions (areas of uniform intensity), thereby emphasizing high spatial frequency components (for instance edges) in the image. The sample is illuminated with light incident on the sample at a high angle that is not collected by the objective lens, unless it is scattered by the imaged object. Even though it is a simple method that provides high-quality images, it usually requires a classic bulky optical microscope, with dedicated objectives and filtering cubes.

Here, we present research aimed at creating a lab-on-chip dark-field imaging device that can provide dark field imaging capabilities without the need for sophisticated equipment. We produce a micro-patterned fluorescent surface with a spatially tunable light emission profile, consisting of quantum dots in a polymer matrix sandwiched between a Bragg reflector on the top and semi-spherical micro-concavities at the bottom. While the quantum dots emit light in all directions, the confinement between the Bragg mirror and the semi-spherical cavities allow only light to exit from the surface in a limited angle range. The color of the emitted light is determined by the quantum dots' emission spectrum, while the stop band of the Bragg reflector imposes directionality. Tuning of the Bragg reflector band-gap, or the combination of Bragg reflectors with different band-gaps, allows for the creation of a rich variety of light emission profiles.

To maximize light emission in the desired limited angle range, an array of bioinspired, hexagonally arranged semi-spherical gold micro-reflectors is used. Each patterned surface measures 1" x 1", and more than 10 Bragg reflectors can be assembled on it, providing the same number of dark-field imaging ring profiles. A sample placed on top of the surface will be illuminated with light of the desired angular distribution only, which for dark-field imaging would be at angles larger than the numerical aperture of the imaging objective. This surface with tailorable light emission profile constitutes a highly compact, simple, tunable solution for dark-field imaging, which could for instance find application in miniaturized imaging devices for microbiology.

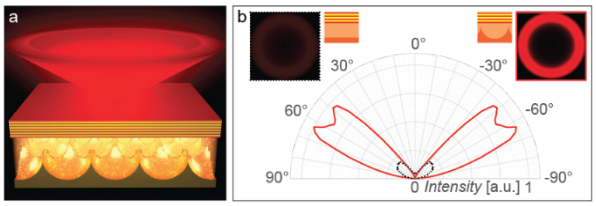

▲ Figure 1: (a) Concept schematic of the emission profile of a dark-field enabling light-emitting surface, (b) calculated angular light emission profile for a substrate with flat bottom surface (black curve and left inset) and a substrate with patterned bottom reflector (red curve and right inset).

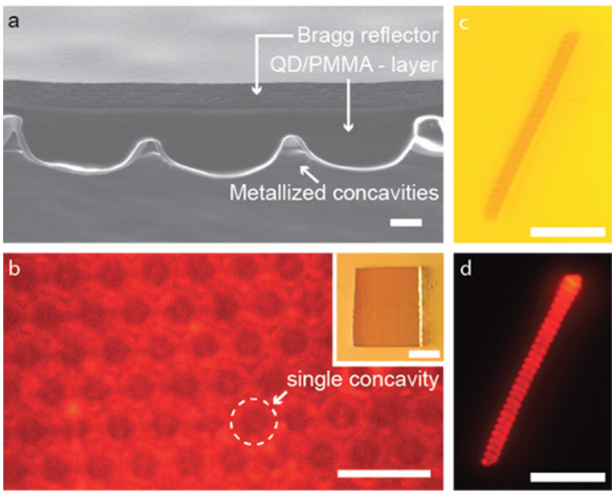

▲ Figure 2: (a) SEM cross-section view of the light-emitting dark-field substrate. Scale bar 1 µm, (b) Top view of the device. Scale bar 10 µm. Inset shows a macroscopic top-view of the assembled system, (c & d) comparison of the microscope images of a marine micro-organism in bright field imaging (c) and surface-enabled dark-field imaging (d); scale bars 20 µm.

FURTHER READING

- M. Kolle, P. M. Salgard-Cunha, M. R. J. Scherer, F. Huang, P. Vukusic, S. Mahajan, J. J. Baumberg, and U. Steiner, "Mimicking the Colourful Wing Scale Structure of the Papilio Butterfly," *Nature Nanotechnology*, vol. 5, no. 7, 511-515, 2010.

See-Through Light Modulators for Holographic Video Displays

S. Jolly, N. Savidis, B. Datta, V. M. Bove, Jr.
Sponsorship: MIT Media Lab Research Consortium, AFRL

In this research (a collaboration with Dr. Daniel Smalley of Brigham Young University), we design and fabricate acousto-optic, guided-wave modulators in lithium niobate for use in holographic and other high-bandwidth displays. Guided-wave techniques make possible the fabrication of modulators that are higher in bandwidth and lower in cost than analogous bulk-wave acousto-optic devices or other spatial light modulators used for diffractive displays; these techniques enable simultaneous modulation of red, green, and blue light. In particular, we are investigating multichannel variants of these devices with an emphasis on maximizing the number of modulating channels to achieve large total bandwidths. To date, we have demonstrated multichannel full-color modulators capable of displaying holographic light fields at standard-definition television resolution and at video frame rates. Our current work explores a device architecture suitable for wearable augmented reality displays and other see-through applications, in which the light outcouples toward the viewer (Figure 1), fabricated using femtosecond laser micromachining (Figure 2).

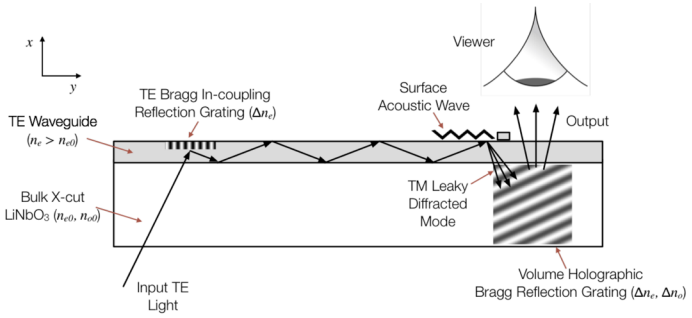

▲ Figure 1: Diagram of near-eye version of our device.

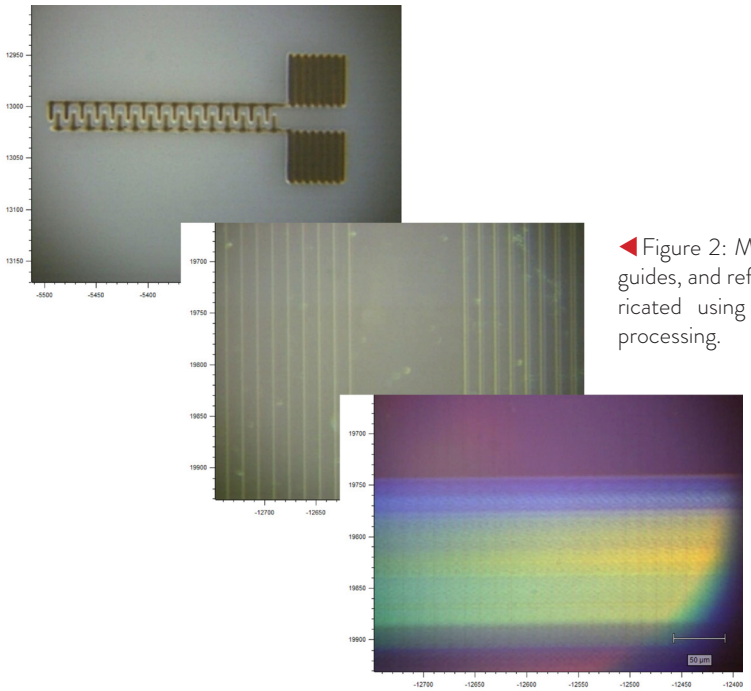

◀ Figure 2: Metal features, waveguides, and reflection gratings fabricated using femtosecond laser processing.

FURTHER READING

- S. Jolly, N. Savidis, B. Datta, D. Smalley, and V. M. Bove, Jr., "Near-to-Eye Electroholography via Guided-Wave Acousto-Optics for Augmented Reality," *in Proc. SPIE Practical Holography XXXI: Materials and Applications*, 10127, 2017.
- B. C. Datta, N. Savidis, M. Moebius, S. Jolly, E. Mazur, and V. M. Bove, Jr., "Direct-Laser Metal Writing of Surface Acoustic Wave Transducers for Integrated-Optic Spatial Light Modulators in Lithium Niobate," *in Proc. SPIE Advanced Fabrication Technologies for Micro/Nano Optics and Photonics X*, 10115, 2017.
- N. Savidis, S. Jolly, B. Datta, M. Moebius, T. Karydis, E. Mazur, N. Gershenfeld, and V. M. Bove, Jr., "Progress in Fabrication of Waveguide Spatial Light Modulators via Femtosecond Laser Micromachining," *in Proc. SPIE Advanced Fabrication Technologies for Micro/Nano Optics and Photonics X*, 10115, 2017.

Atomic Color Centers in Wide-Bandgap Semiconductors

B. Lienhard, G. Grosso, H. Moon, T. Schröder, K.-Y. Jeong, S. Mouradian, T.-J. Lu, I. Aharonovich, D. Englund
Sponsorship: NSF CIQM, ARL-CDQI, U.S. Department of Energy: Basic Energy Sciences

Atoms and atom-like emitters play central roles in many areas of quantum information processing, including using them as single-photon sources, nonlinearities, and quantum memories. In recent years, there has been tremendous progress in developing quantum emitter systems based on crystallographic defects in wide-bandgap semiconductors. The interest in solid-state quantum emitters started with in diamond embedded nitrogen vacancy (NV) color centers, which have well-defined optical transitions as well as electronic spin states that can be controlled optically or by microwave radiation. They represent prime systems for solid-state quantum technologies including quantum repeaters, nanoscale sensors, single-photon nonlinearities, and single-photon sources.

Single-crystal silicon carbide (SiC) is another wide-bandgap semiconductor with wider industrial applications than diamond in optoelectronics, high power electronics, and microelectromechanical systems. Recently, we identified a single-photon emitter in 4H-SiC in the visible spectrum, illustrated in Figure 1a. The emitter is photostable at both room and low temperatures and enables 2 million photons per second, shown in Figure 1b. Furthermore, cryogenic measurements reveal a narrow zero phonon line with a linewidth ~0.1 nm that accounts for more than 30% of the total photoluminescence spectrum.

Another emergent material for quantum memories and quantum emitters is layered 2-D materials. They have also recently been shown to host a range of single-photon emitters. Demonstration of quantum emission in 2-D hBN now broadens its appeal for quantum information processing applications. Atom-like defects in hBN confine electronic levels within the extremely wide band gap (5.955 eV) and result in photostable and surprisingly robust emitters with single-photon emitter characteristics. The emission energy of these emitters spans a large spectral band, limiting individual emitter indistinguishability. Recently, we were able to improve optical properties, indicated in Figure 1c, and demonstrated spectral tuning of such hBN emitters. The tunability promises the generation of many quantum emitters with frequency-matched emission.

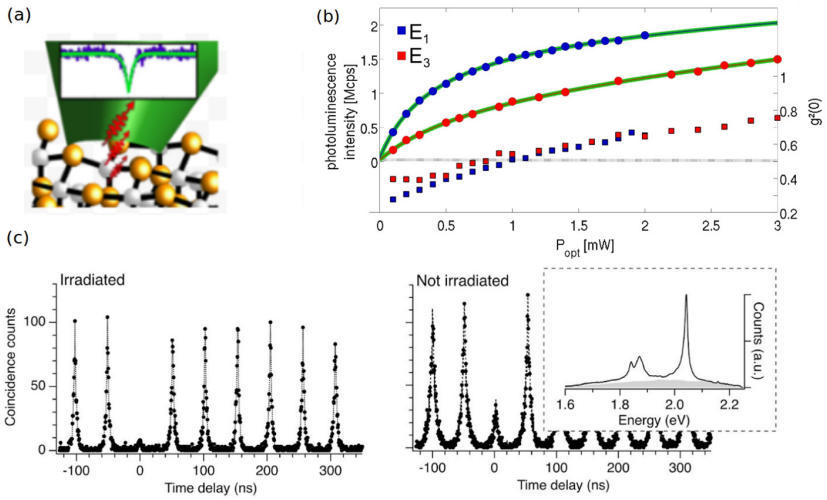

▲ Figure 1: (a) Schematic of single-photon emitter (SPE) in silicon carbide, (b) intensity and single-photon emission purity measurement of SPE in silicon carbide, (c) pulsed second-order autocorrelation histograms in purified (irradiated) and untreated area of SPE in hexagonal boron nitride. Inset shows a spectrum indicating the sum of the spectral components of the SPE (black) and background (gray).

FURTHER READING

- I. Aharonovich, D. Englund, and M. Toth, "Solid-State Single-Photon Emitters," *Nature Photonics*, vol. 10, no. 10, 631–641, 2016.
- B. Lienhard, T. Schröder, S. Mouradian, F. Dolde, T. T. Tran, I. Aharonovich, and D. Englund, "Bright and Photostable Single-Photon Emitter in Silicon Carbide," *Optica*, vol. 3, no. 7, 768, 2016.
- G. Grosso, H. Moon, B. Lienhard, S. Ali, D. K. Efetov, M. M. Furchi, P. Jarillo-Herrero, M. J. Ford, I. Aharonovich, and D. Englund, "Tunable and High Purity Room-Temperature Single Photon Emission from Atomic Defects in Hexagonal Boron Nitride," *arXiv*:1611.03515, 2016.

Self-Aligned Local Electrolyte Gating of 2-D Materials with Nanoscale Resolution

C. Peng, D. K. Efetov, S. Nanot, R.-J. Shiue, G. Grosso, Y. Yang, M. Hempel, P. Jarillo-Herrero, J. Kong, F. Koppens, D. Englund
Sponsorship: ONR, MIT Lincoln Laboratory

A central challenge in making 2-D material-based devices faster, smaller, and more efficient is to control their charge carrier density at the nanometer scale. Traditional gating techniques based on capacitive coupling through a gate dielectric cannot generate strong and uniform electric fields at this scale due to divergence of the fields in dielectrics. This field divergence limits the gating strength, boundary sharpness, and pitch size of periodic structures and restricts possible geometries of local gates (due to wire packaging), precluding certain device concepts, such as plasmonics and transformation optics based on metamaterials.

Here we present a new gating concept based on a dielectric-free, self-aligned electrolyte technique that allows spatial modulation of charges with nanometer resolution. We employ a combination of a solid-polymer electrolyte gate and an ion-impenetrable e-beam-defined resist mask to locally create excess charges on top of the gated surface. Electrostatic simulations indicate high carrier density variations Δn = 1014 cm-2 across a length of 10 nm at the mask boundaries on the surface of a 2-D conductor, resulting in a sharp depletion region and a strong in-plane electric field of 6×10^8 V/m across the so-created junction.

We apply this technique to the 2-D material graphene to demonstrate the creation of tunable p-n junctions for optoelectronic applications. We also demonstrate the spatial versatility and self-aligned properties of this technique by introducing a novel graphene thermopile photodetector in the mid-infrared.

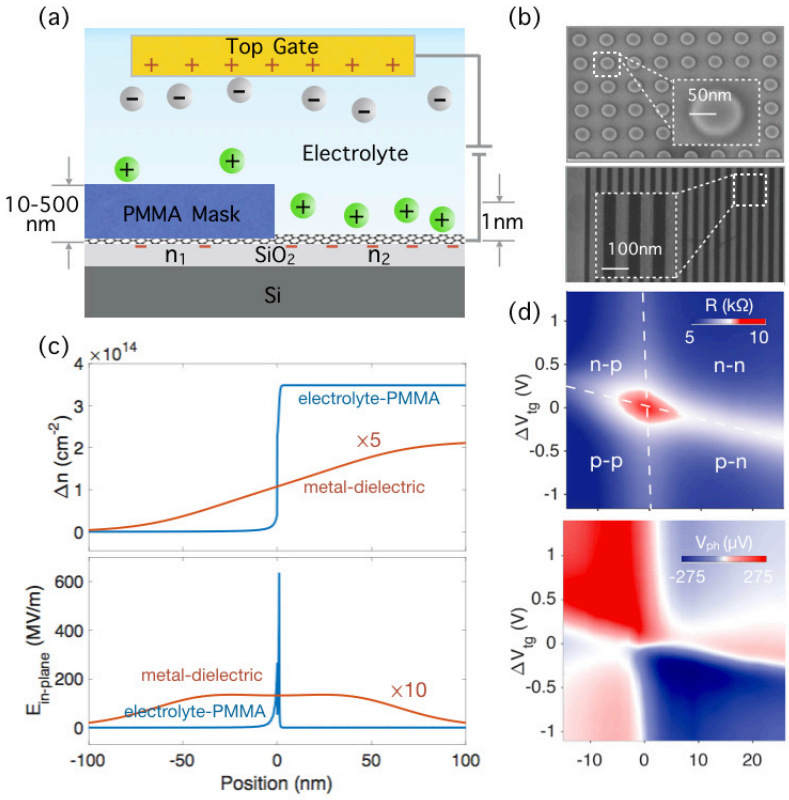

◀ Figure 1: (a) Geometry and working principle of nanoscale electrolytic doping of 2-D materials with PMMA screening mask. n_1 and n_2 denote charge carrier densities in mask-protected region and exposed region, respectively, (b) simulated charge carrier density n profile and in-plane electric field intensity $E_{in-plane}$ for single junction, compared between proposed electrolyte-PMMA-mask gating and metal-dielectric split gating schemes, (c) scanning electron micrographs of fabricated PMMA masks on graphene with nanoscale dimensions. (d) Resistance R and photovoltage V_{ph} as function of V_{tg} and V_{bg}, measured at p-n interface created by PMMA-electrolyte doping technique.

FURTHER READING

- C. Peng, D. K. Efetov, S. Nanot, R.-J. Shiue, G. Grosso, Y. Yang, M. Hempel, P. Jarillo-Herrero, J. Kong, F. H. L. Koppens, and D. Englund, "*Self-Aligned Local Electrolyte Gating of 2D Materials with Nanoscale Resolution*," arXiv:1610.07646, 2016.
- D. K. Efetov and P. Kim, "Controlling Electron-Phonon Interactions in Graphene at Ultrahigh Carrier Densities," *Physical Review Lett.*, vol. 105, no. 25, 256805, 2016.
- D. Huigao, D. Winston, J. K. W. Yang, B. M. Cord, V. R. Manfrinato, and K. K. Berggren, "Sub-10-nm Half-Pitch Electron-Beam Lithography by using Poly (Methyl Methacrylate) as a Negative Resist," *J. Vacuum Science & Technology B, Nanotechnology and Microelectronics: Materials, Processing, Measurement, and Phenomena*, vol. 28, no. 6, C6C58-C6C62, 2010.

Flexible Chalcogenide Glass Waveguide Integrated Photodetectors

L. Li, H. Lin, J. Michon, Y. Huang, J. Li, C. Smith, K. Richardson, J. Hu

Flexible photodetectors are important components for imaging, communications, and sensing applications. Traditional photodetectors are typically made on rigid semiconductor substrates and couple to incident light via free space. Here we present an experimental demonstration of waveguide coupled flexible photodetectors. By taking advantage of the substrate-blind integration capacity of chalcogenide glass photonic components, high index contrast glass optical waveguides were monolithically integrated on InGaAs nanomembrane metal semiconductor metal photodetectors hybrid-bonded to flexible substrates (Figure 1a-b).

To monitor the photodetector response, we have assembled the measurement setup shown in Figure 1c. A pair of motion stages was used to control the bending of the flexible detector, and another two tapered lens-tip fibers were used to couple light from a laser into and out of the waveguides. Two micro-probes were used to detect the electrical response. Figure 1d plots the current-voltage (I-V) curves of the detector measured in the dark and under illumination with 250-μW incident optical power at 1550-nm wavelength. The device shows a negligible saturation dark current of 0.5 nA at 10 V bias. The photocurrent increases linearly with increasing optical power, as shown in Figure 1e. Slope of the response curve yields a responsivity of 0.5 A/W at 1550 nm, corresponding to an external quantum efficiency of 40%. Further, the dark current and photo response of the device remain unchanged with bending radii down to 0.7 mm, which represents a significant improvement in mechanical flexibility over previously demonstrated semiconductor NM photodetectors (Figure 1f-g).

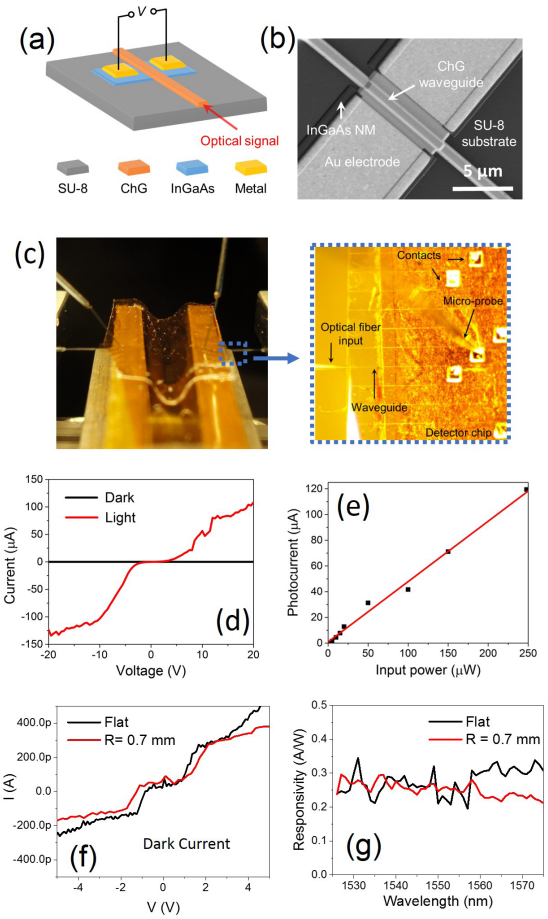

▲ Figure 1 Waveguide integrated flexible detectors. (a) Schematic diagram of the glass waveguide-integrated photodetector, (b) SEM micrograph of a detector, (c) photo of the testing setup, (d) I-V response of the detector in the dark and under illumination, (e) photocurrent of the detector as a function of input optical power in the waveguide, (f) I-V response in the dark under flat and bending condition, (g) spectral response of the detector at -5 V bias under flat and bending condition.

FURTHER READING

- L. Li, H, Lin, J. Michon, Y. Huang, J. Li, Q. Du, A. Yadav, K. Richardson, T. Gu, and J. Hu, "A New Twist on Glass: a Brittle Material Enabling Flexible Integrated Photonics," *Int. J. Appl. Glass Sci.*, doi:10.1111/ijag.12256, 2016.
- L. Li, H. Lin, S. Qiao, Y. Zou, S. Danto, K. Richardson, J. D. Musgraves, N. Lu, and J. Hu, "Integrated Flexible Chalcogenide Glass Photonic Devices," *Nat. Photonics*, vol. 8, 643-649, 2014.

Monolithically Integrated Glass on Two-Dimension Materials Photonics

H. Lin, Y. Song, Y. Huang, D. Kita, S. Deckoff-Jones, K. Wang, L. Li, J. Li, H. Zheng, Z. Luo, H. Wang, S. Novak, A. Yadav, C. Huang, R. J. Shiue, D. Englund, T. Gu, D. Hewak, K. Richardson, J. Kong, J. Hu

Two-dimensional (2-D) materials are of tremendous interest to integrated photonics given their singular optical characteristics spanning light emission, modulation, saturable absorption, and nonlinear optics. The current approach to integrating 2-D materials with photonic devices generally relies on transferring these atomically thin crystals onto prefabricated photonic components, which limits the yield and fully utilizing their capabilities. To resolve these issues, an alternative integration route entails growing an optically thick chalcogenide glass (ChG) film directly on 2-D materials and lithographically patterning it into functional photonic devices. Figure 1a displays the Raman spectra of monolayer CVD graphene before and after coating with a 450-nm- thick ChG film. No defect-related peaks (D, D' or D+G) were observed after ChG deposition, indicating that the low-temperature glass deposition does not introduce structural defects into graphene. We further confirm that the structures of other 2-D materials (MoS2, black phosphorus, InSe, and hexagonal BN) likewise remain intact after ChG deposition.

Such integration compatibility not only leads to a bottom-up process to fabricate mid-IR photodetectors (Figures 1b and 1g) or modulators, but also facilitates the fabrication of unconventional multi-layer structures incorporating 2-D materials to optimally engineer their interactions with the optical mode. As an example, we exploit the giant optical anisotropy of graphene and modal symmetry in graphene-sandwiched waveguides to demonstrate an ultra-broadband polarizer (Figure 1c and 1e) and a thermo-optic switch with energy efficiency an order of magnitude higher than previous reports (Figures 1d and 1f). In addition, the insulating ChG can function as a gate dielectric. We harness this feature to demonstrate the first mid-IR graphene waveguide modulator (Figure 1h). We foresee that the versatile glass-on-2D-material platform will significantly expedite and expand integration of 2-D materials to enable new photonic functionalities.

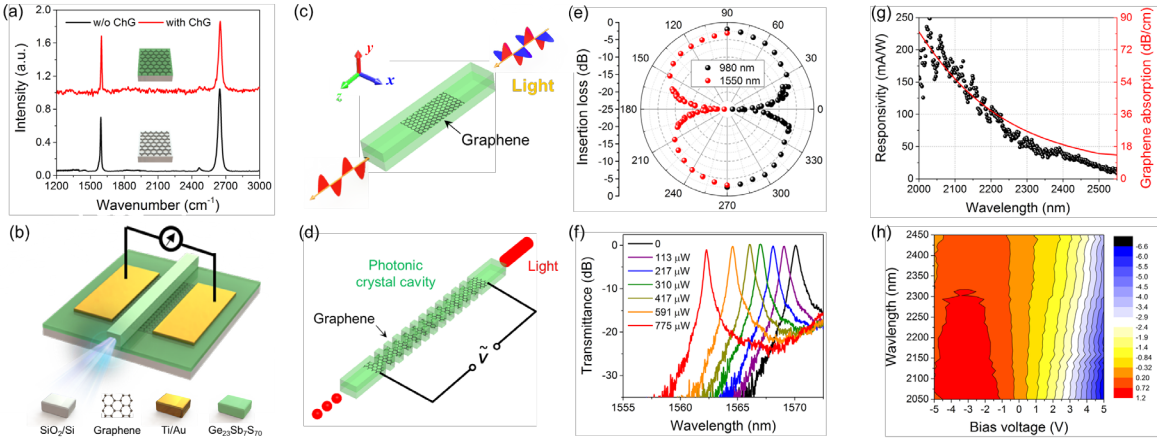

▲Figure 1: (a) Raman spectra of as-transferred monolayer CVD graphene (black) and graphene covered with a $Ge_{23}Sb_7S_{70}$ glass layer (red), schematic diagrams of (b) mid-IR waveguide-integrated detector, (c) graphene-sandwiched waveguide polarizer, and (d) photonic crystal thermo-optic switch, (e) polar diagram showing the polarizer performance at 980-nm and 1550-nm wavelengths, (f) optical transmission spectra of the switch at varying input power levels into the graphene heater, (g) mid-IR broadband spectral dependences of the detector's responsivity (at 1.5 V bias) and calculated optical absorption in the graphene layer, and (h) measured color contour maps showing wavelength and bias dependent modulation depth of the device in dB/mm (relative to its transmittance at zero bias).

FURTHER READING

- H. Lin, Y. Song, Y. Huang, D. Kita, K. Wang, L. Li, J. Li, H. Zheng, S. Deckoff-Jones, Z. Luo, H. Wang, S. Novak, A. Yadav, C. Huang, T. Gu, D. Hewak, K. Richardson, J. Kong, and J. Hu, "Chalcogenide Glass-on-Graphene Photonics" [submitted] *Physics Optics*, arXiv:1703.01666.

Broadband Optical Phase Change Materials and Devices

Y. Zhang, J. Li, J.B. Chou, Z. Fang, A. Yadav, H. Lin, Q. Du, J. Michon, Z. Han, Y. Huang, H. Zheng, T. Gu, V. Liberman, K. Richardson, J. Hu
Sponsorship: DoD

Optical phase change materials (O-PCMs) are a class of materials that exhibit extraordinarily large optical property change (e.g., index change $\Delta n > 1$) when undergoing a solid-state phase transition. These materials, such as Ge-Sb-Te (GST) compounds, have been exploited for a plethora of optical applications including optical switching, reconfigurable metasurface, and non-volatile display. Traditional phase change materials, however, generally suffer from large optical losses even in their dielectric states. The large optical losses fundamentally limit the performance of photonic devices based on traditional O-PCMs.

Here we report the synthesis, characterization and device integration of a new class of O-PCMs, Ge-Sb-Se-Te (GSST) alloys. A series of GSST thin films with the compositions of $Ge_2Sb_2Se_xTe_{5-x}$ (x = 1, 2, 3, 4, and 5) were prepared using thermal evaporation. We experimentally validated that Se substitution for Te results in an increase in the optical band gap, enabling low loss operation in the telecommunication bands (Figure 1a and 1b). Meanwhile, the GSST materials claim reduced free carrier concentrations and mobility compared to GST, which effectively suppresses free carrier absorption in the infrared. Figure 1c shows that the $Ge_2Sb_2Se_4Te_1$ (GSS_4T_1) material features broadband transparency covering 1 micron to the long wave infrared (LWIR). The low optical loss of the GSS_4T_1 alloy leads to an exceptionally better performance than $Ge_2Sb_2Te_5$ (GST 225).

We deposited and patterned GSST and GST pads on SiN micro-ring resonators. Figure 1e and 1f plot the transmittance spectra of micro-ring devices integrated with the GST 225 and the GSS_4T_1 O-PCMs when they are switched from amorphous to crystalline state. The device integrated with the GSS_4T_1 material claims a large on/off contrast ratio of 41 dB and an insertion loss of 0.2 dB, both of which represent significant improvements compared to state-of-the-art GST-based devices.

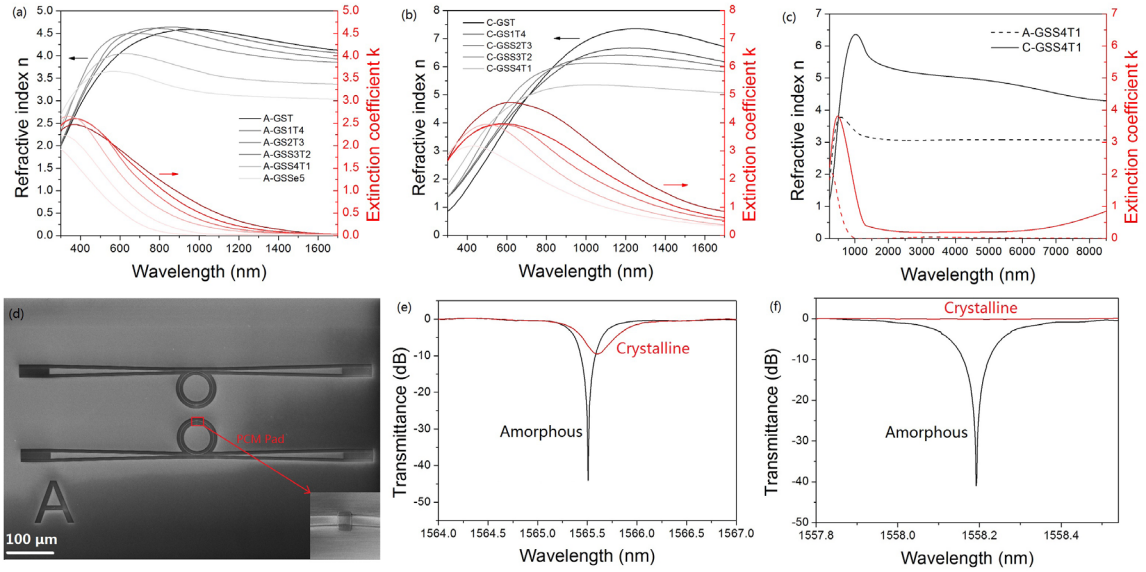

▲Figure 1: (a & b) optical properties of (a) amorphous and (b) crystalline GSST alloys, (c) optical properties of amorphous (dashed lines) and crystalline (solid lines) GSS_4T_1 from the visible to LWIR, (d) SEM images of fabricated devices, (e & f) transmission spectra of (e) GST-based and (f) GSS_4T_1-based devices.

FURTHER READING

- M. Rudé, J. Pello, R. E. Simpson, J. Osmond, G. Roelkens, J. J. van der Tol, and V. Pruneri, "Optical Switching at 1.55 Mm in Silicon Racetrack Resonators using Phase Change Materials," *Appl. Phys. Lett.*, vol. 103, 1, 41119, 2013.
- C. Ríos, M. Stegmaier, P. Hosseini, D. Wang, T. Scherer, C. D. Wright, H. Bhaskaran, and W. H. Pernice, "Integrated All-Photonic non-Volatile Multi-Level Memory," *Nat Photonics*, vol. 9, 725-732, 2015.

High-Performance Inorganic CsPbBr3 Perovskite Light-Emitting Diodes by Dual Source Vapor Deposition

S. Xie, A. Osherov, V. Bulović
Sponsorship: U.S. Department of Energy EFRC

Organometal halide-based perovskites, with the typical chemical formula ABX_3, have emerged as a promising class of semiconducting materials for thin-film optoelectronics in the past few years. Those semiconductors possess unique electro-optical properties, such as long-range carrier diffusion length, high absorption coefficients, and low levels of defect states, yielding solar cells with over 20% power conversion efficiency. While many of the research efforts have been captivated by the potential of their photovoltaic applications, perovskites are nonetheless promising light emitters. Indeed, color-tunable electrically-driven perovskite light-emitting diodes (PeLEDs) have tremendous potential for novel display and lighting applications. In addition to its bright photoluminescence (PL) and excellent wavelength tunability, $CsPbX_3$ (X=I, Br, Cl) in particular exhibits superior thermal and chemical stabilities when compared to organic-inorganic analogs such as $CH_3NH_3PbX_3$.

Unfortunately, low solubility limits of CsBr precursor hinder the fabrication of a dense, compact $CsPbBr_3$ layer with complete coverage and smooth morphology via solution processing. Incomplete coverage of perovskite emitting layers results in substantial leakage current that has limited the luminescent efficiency of previously reported cesium-based PeLEDs. Physical vapor deposition of fully inorganic $CsPbX_3$ perovskites offers a scalable alternative to solution processing. In this work, we report a systematic approach for preparation of highly efficient $CsPbBr_3$ PeLEDs using vacuum deposition. Fabrication of $CsPbBr_3$ thin films with complete surface coverage and reduced roughness in addition to precise control over the film thickness and stoichiometry is demonstrated. Perovskite films are optimized for the best device performance by varying parameters including evaporation rate, film thickness, and composition of the as-deposited perovskite layer. As a result, $CsPbBr_3$-based PeLEDs that exhibit narrow green emission significantly reduced leakage current; therefore, substantially improved brightness and efficiency were realized.

Multilayer Thin Films for Hot Carrier Filtering and Spectroscopy

Z. J. Tan, N. X. Fang

Hot carriers are electrons or holes not in thermal equilibrium with its lattice. They can be generated electrically by injection through a barrier layer or optically from plasmonic excitations. These hot carriers can have useful large excess energy of several eVs much larger than the energy which can be supplied thermally under practical conditions.

However, it is difficult to harvest the full potential of these hot carriers due to their fast thermalization times. Furthermore, there is very little insight into how one can control or measure the energy profile of these hot carriers due to the lack of robust experimental techniques that can probe these carriers before thermalization sets in.

We perform simulations to show that the use of multilayer dielectric films can be used as bandpass filters to retrieve the energy profile of hot carriers (see Figures 1 and 2). The measured electrical current through a crossbar structure separating such a stack of dielectric film can be inverted to deduce the initial energy profile of generated hot carriers because hot carriers with different energies have different transmissions across the barriers. Existing work with hot carrier filtering uses only single layer oxides. We show that a dual layer TiO_2/Al_2O_3 stack has a high discriminatory power for hot carrier spectroscopy.

We are fabricating devices to compare with our theoretical predictions. In our device, optical generation of hot carriers is optimized by choosing the material and thickness of the metal terminal to increase absorptivity at 405 nm. Joint density-of-state calculations show that highly energetic hot electrons can be produced in Au beyond an illumination energy threshold of 3 eV. We intend to use our multilayer dielectric films to perform energy spectroscopy on these hot carriers.

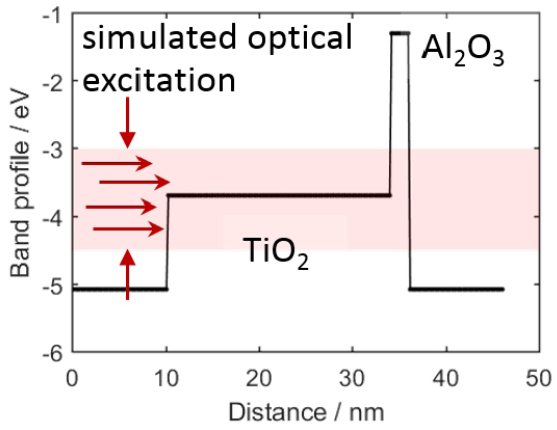

▲Figure 1: Simulated conduction band-edge profile for a TiO_2/Al_2O_3 stack and assuming a uniform profile of optically generated carriers at the source.

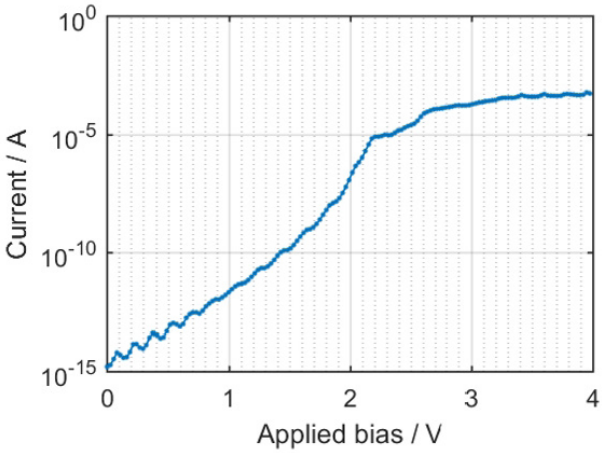

▲Figure 2: The simulated electrical current shows a bend (at 2.2 V) whose properties are dependent on the band profile design and the energy profile of hot electrons are the source. An experimental version of this graph will allow us to deduce the actual energy profile of generated hot carriers.